Asian Journal of Information Technology 5 (11): 1248-1255, 2006
Medwell Journals, 2006

Microstructural and Characteristics Study of Low Voltage ZnO-Bi_2O_3-Based Varistor Doped with Cr_2O_3, SiO_2 and Varying Amounts of Al_2O_3

[1,2]A. Djelloul, [1]A. Boumaza, [3]N. Bouzid, [2]A. Mahdjoub, [2]L. Hadjeris
[1]SETI Centre Universitaire de Khenchela, Algérie
[2]L M S S E F Laboratory Algérie
[3]LPM Laboratory, Université de Ouargla, Algérie

Abstract: ZnO-Bi_2O_3-based varistor samples doped with 2.0 mol% of (Cr_2O_3+SiO_2) and varying amounts of Al_2O_3 in the range from 7.0 to 1.0 mol% were fired at 1200°C for 2h. A new process is described for achieving the current-voltage characteristics of a low voltage ZnO varistor. Second phases, segregated and precipitated in ZnO-based varistors, encountered in triple junctions and grain boundaries regions were identified using XRD, SEM and energy dispersive spectrometry. Using IR spectroscopy we have observed OH and H_2O molecular stretch modes at 3444.24 cm^{-1} with a width of 273.53 cm^{-1} and near 1637.27 cm^{-1} with a width of 42.64 cm^{-1} respectively. The hydrogen in Al doped ZnO-Bi_2O_3-based varistor may have a one site preference, resulting in a wider OH peak. The band at 662 cm^{-1} should be due to the presence of the $ZnAl_2O_4$ spinel, undoubtedly identified in the XRD patterns of sintered ceramics. Addition of hydrogen to aluminium doped varistors slow down the grain growth effect.

Key words: Varistor, microstructure, ZnO, $ZnAl_2O_4$

INTRODUCTION

The ZnO-based varistor is a non-ohmic ceramic component, which has ZnO as the principal ingredient and other oxide additives. Its microstructure is generally known to contain ZnO grains, a Bi_2O_3-rich phase, which plays the role of an intergranular layer and spreadingly distributed spinel-and/or pyrochlore-type phases.

The voltage-current relationship above the turn-on voltage can approximated by the equation: $I = KV^{\alpha}$, where K is dependent on the device geometry and α defines the degree of nonlinearity in the resistance. This simple formula has been accepted to describe the fact that from some threshold voltage, the current increases abruptly with little change in the applied voltage. This has lead to the wide application of ZnO-based varistors in surge arresters. The study of non-linear current-voltage characteristics of ZnO based varistors, as well as of its degradation in service, is of great technological importance[1,2]. The understanding and modeling of these phenomena need the knowledge of the defect structure in ZnO. However, the defect chemistry in ZnO is not well established yet.

However, an important characteristic of ZnO-based varistors is their high breakdown voltage (~ 3.6 V per grain boundary) which precludes them for low voltage applications[1]. Alumina is very effective in enhancing varistor grain growth and thus reducing breakdown voltage[3].

The purpose of this work is to investigate the effect of Al_2O_3 incorporation on microstructure of ZnO-Bi_2O_3-Al_2O_3-Cr_2O_3-SiO_2 (in short ZBACS)-based varistors.

MATERIALS AND METHODS

Reagent grade (>99.8%) powders of ZnO, Bi_2O_3, Al_2O_3, Cr_2O_3 and SiO_2 were used as starting materials. All the powders, except Bi_2O_3, were mixed in a ball-milled reactor in deionised water using zirconia beads as the dispersion agent. After this the samples were dried and at the end one adds the bismuth oxide. Compositions of ZnO varistors were summarized in Table 1. In each batch mixture the amounts of the respective oxide additives except ZnO and Al_2O_3 were kept 1 mol%; those of Al_2O_3 added to balance oxides were 1, 2, 3, 5 and 7 mol%, of which batches were abbreviated as Al1, Al2, Al3, Al5 and Al7, respectively. Powder mixtures were uniaxially pressed under 200 MPa into disks of 12 mm in diameter and 2.5 mm thick. Sintering was conducted at 1200°C for 2 h. The heating and cooling rate was 5°C min^{-1}.

Corresponding Author: A. Djelloul, SETI Centre Universitaire de Khenchela, Algérie

Table 1: Composition of Zno veristors

Sample name	Al_2O_3 (mol%)	ZnO+Bi_2O3+Cr_2O_3+SiO_2 (mol%)
Al1	1	96.00+01.00+01.00+01.00
Al2	2	95.00+01.00+01.00+01.00
Al3	3	94.00+01.00+01.00+01.00
Al5	5	92.00+01.00+01.00+01.00
Al7	7	90.00+01.00+01.00+01.00

Specimen densities were determined from weight and dimension measurements. For microstructure analysis, sintered products were ground and polished down to 1.0 μm diamond paste. The size of the final samples was about 11 mm in diameter and 2.0 mm in thickness. Silver paste was coated on both faces of the samples and the ohmic contact of electrodes was formed by heating at 600°C for 30 min. The size of electrodes was 10 mm in diameter.

The DC voltage-current (V-I) characteristics of ZnO varistors were measured by stepping up the linear stair voltage in increment of 0.5 V using a programmable Keithley 237 unit. To avoid joule heat of varistors, the varistors were applied up to 50 mA cm^{-2}. The varistor voltage ($V_{1\ mA}$) was measured at 1.0 mA cm^{-2} and the leakage current (I_L) was defined as the current at 0.83 $V_{1\ mA}$. In addition, the nonlinear exponent (α) is defined from $\alpha = 1/(\log E_2 - \log E_1)$, where E_1 and E_2 are the electric fields corresponding to 1.0 mA cm^{-2} and 10 mA cm^{-2}, respectively.

FTIR spectra for Al doped ZBACS-based varistors were recorded on Jasco 460 PLUS FTIR spectrometer in the range 4000-400 cm^{-1} following KBr pellet technique at 300 K with a scanning speed of 3 mm sec^{-1}. SEM analysis was conducted using an TS5130MM microscope. The compositional analysis of the selected areas was determined by an attached X-ray energy dispersive spectroscopy system. The structural analysis of the ZBACS-based varistors doped with Cr_2O_3, SiO_2 and varying amounts of Al_2O_3 is done by powder X-ray diffraction (XRD) data collected on a Seifert XRD 3003-TT diffractometer using Cu-Kα radiation.

RESULTS AND DISCUSSION

Extra peaks, in addition to those of the main ZnO matrix phase (JCPDS card number 05-0664), were visible in XRD patterns of sintered ceramics, Fig. 1. According to ICDD cards *-Marks attributed to A-$ZnAl_2O_4$ spinel phase (JCPDS card number 05-0669), B-Bi rich phase (α-Bi_2O_3) (JCPDS card number 14-0699, 06-0307), D-$ZnCrO_4$ phase (JCPDS card number 19-1456). Changing the amount of Al_2O_3 produced noticeable change in XRD data Fig. 1.

SEM and X-ray mapping of the samples confirmed that the varistor samples had a morphology in which

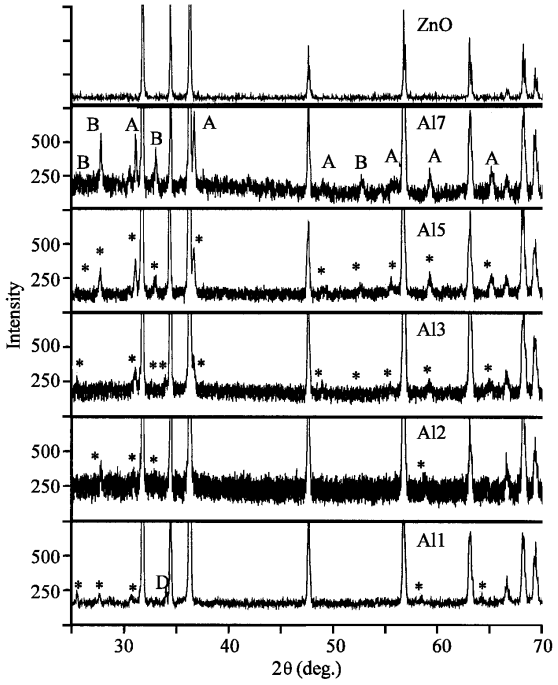

Fig. 1: XRD of samples sintered at 1200°C for 2h (*indicates extra peaks), *attributed to A-$ZnAl_2O_4$ spinel phase, B-Bi rich phase (α-Bi_2O_3), D-$ZnCrO_4$ phase

Fig. 2: SEM results in backscattered electron mode of ZBACS-based varistors sintered at 1200°C for 2h with 5 mol% of Al_2O_3 content

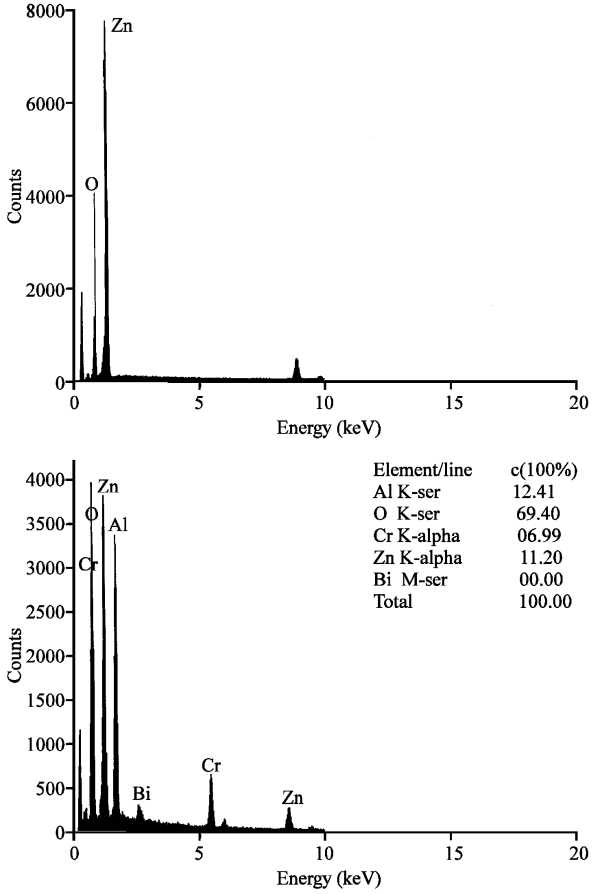

Fig. 5: EDS analysis of ZBACS-based varistors, sintered at 1200°C for 2h with 2 mol% of Al_2O_3 content, X and Y-marked region, from the top to the bottom, respectively

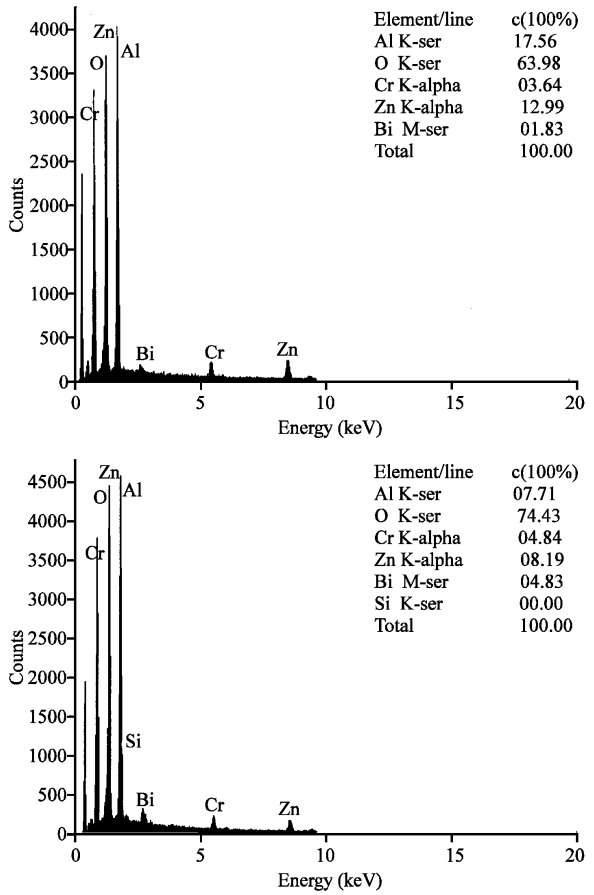

Fig. 6: EDS analysis of ZBACS-based varistors, sintered at 1200°C for 2h with 7 mol% of Al_2O_3 content, Y and Z-marked region, from the top to the bottom, respectively

Bismuth was found at triple junctions and grain boundaries, whereas the Aluminium was distributed uniformly throughout the samples. Fig. 2 and 3 shows a SEM micrograph and in detail the X-Y-Z-marked region of the polished samples Al2 and A17, respectively of the Z BACS-based varistors sintered at 1200°C for 2h with Al_2O_3 content. The X, Y and Z marks indicate the specific regions to qualitative EDS analyses (Fig. 2 and 3), denoting, respectively, a ZnO grain, a large round-like precipitate and a nearby matrix with fine precipitates, whose EDS patterns are shown, respectively, in the Fig. 4, 5 and 6.

To identify the precipitates in the agglomerates, the experiments were carried out in the SEM using X-ray microanalysis conducted with Energy Dispersive Spectrometry (EDS) at 20 kV. Large agglomerates of particles visible on surface of sample, in backscattered electron mode. It revealed a large concentration of Al as well as the presence of Bi, Cr and Zn. An example is given in Fig. 2 and 3, showing an agglomerate as well as spectra, taken at 20 kV in Fig. 4 and 5, of a large round-like precipitate (dark, Y-marked) and of a nearby matrix with fine precipitates (white, Z-marked). More detailed microanalysis revealed that at least two types of oxides are present in the agglomerates, i.e., the majority containing from 12 to 18 at% Al, up to 2 at% Bi, plus Cr and Zn (Y-marked) and the minority containing about 8 at% Al, up to 5 at% Bi, Cr and Zn (Z-marked). XRD and SEM analyses were used to reveal the differences between the various Bi_2O_3 phases. Most of Bismuth oxide in the samples Al1, Al2 and Al3 may be is under its amorphous phase, whereas in Al5 and Al7 is in its crystalline phase. Figure 2 and 3 (micrographs of the centre) compare the microstructures of Al2 and Al7, respectively. Alumina markedly affects the microstructure, leading to the formation of large, elongated ZnO grains in

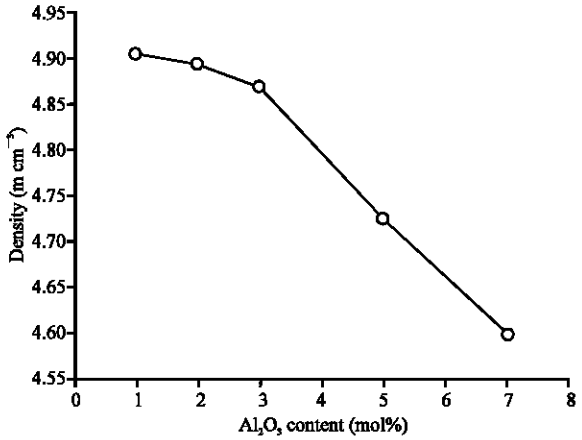

Fig. 7: Density of ZBACS-based varistors samples sintered at 1200°C for 2 h with Al_2O_3 content

Al7 sample. Observed microstructures show that the $ZnAl_2O_4$ spinel phase grow around alumina by the diffusion of Zn^{2+} in $ZnAl_2O_4$, in agreement with previous results[4].

Since the density of ZnAl2O4 spinel (~ 4.6 g cm^{-3}) is less than the average density of ZnO (~ 5.68 g cm^{-3}). The sintered microstructure was less densified due to the increase of the fraction of $ZnAl_2O_4$ spinel phase as Al_2O_3 content increase and the increases in porosity which assigned to the evaporation of Bi_2O_3 during the liquid phase. The density of ceramics was decreased gradually from 4.90 to 4. 59 g cm^{-3} corresponding to 84.7-79.4% of theoretical density of ZnO.

Figure 7 shows FTIR spectra of varistor samples. The infra-red analysis reveals that the OH contents in the samples are important, which supports the viscous flow of material while slowing down the reactions of condensation which weld the grains of ZnO between them. The OH contents in the samples Al1, Al2 and Al3 are much weaker than in the samples Al5 and Al7. Fourier Transform Infrared experiments with hydrogen on ZnO surfaces are usually made on powders. Two main absorption peaks have been assigned to dissociatively absorbed H_2: the first is the OH vibration peak at 3510 cm^{-1} and the second is the ZnH peak at 1710 cm^{-1}[5]. Previous studies have also shown that hydrogen acts as a shallow donor[6-8] and may be an important element in the growth and processing of n-type ZnO. In addition to hydrogen donors, hydrogen-vacancy complexes have been observed with LVM spectroscopy[9]. It has been shown that hydrogen diffusion[10,11] into zinc oxide (ZnO) will form an OH complex that is observable via a Local Vibrational Mode (LVM) at 3336.8 cm^{-1} at room temperature[12] and H_2O molecular absorbance peak at 1645 cm^{-1}. The total dissolved water concentrations were determined from the intensity of the broad band at 3440 cm^{-1}, which contains the fundamental OH stretching vibrations of both molecular H_2O, ZnOH structural groups. Virtually all H_2O dissolved as OH at all temperatures. The dissolved H_2O is present in ZBACS samples, both as OH groups and in molecular form, the ratio of OH/H_2O is constant (~3.6) for all samples. At high temperature the equilibrium favours the formation of OH by means of the reaction $H_2O+O = 2OH$. On the other hand at low temperature the equilibrium favours the formation of OH by means of the reaction $H_2O = OH+H$.

At room temperature the absorption peaks of OH and H_2O molecular is clearly visible in the samples at 3444.24 cm^{-1} with a width of 273.53 cm^{-1} and near 1637.27 cm^{-1} with a width of 42.64 cm^{-1} respectively. The H_2O molecular absorbance peak was significantly weaker than the OH peak. It is noted that hydrogen in the ZBACS-based varistors may have a one site preference, resulting in a wider OH peak. If the line width of this band (about 273.53 cm^{-1}) were exclusively due to lifetime broadening, the lifetime τ of the bonded species could be estimated using the Heisenberg uncertainty relation $\Delta e\tau = h/2\pi$, where E is energy and h is the Planck constant Fig. 8(a-e). This yields a lifetime of the bonded state on the order of 1.96×10^{-14}, i.e., a lifetime comparable with two vibrational period of the OH group. The band at 662 cm^{-1} should be due to the presence of the $ZnAl_2O_4$ spinel, undoubtedly identified in the XRD patterns of sintered ceramics. The intensity of this shoulder decreases as the alumina content is decreased.

Addition of hydrogen to aluminium doped varistors slow down the grain growth effect. Hydrogen is capable of substituting for zinc in the ZnO lattice and thus appears able to compensate the aluminium content. It is noted that hydrogen and alumina levels should be kept low, in order to prevent excessive donor formation in the ZnO lattice, which can adversely affect electrical properties.

Figure 9a shows I-V characteristics of the specimens sintered at 1200°C. The data are presented in electric field (V/cm)-current density (A cm^{-2}) relation. It is clearly shown that the breakdown curve shifts to higher electric field region with increasing Al_2O_3 content of the specimens. In Fig. 9b the current-voltage data for Al5 and Al7 samples showing high nonlinearity and good reproducibility. These varistors breakdown voltage at around 22 V with an average nonlinearity coefficient α about 10 for Al5 and about 17 for Al7 sample over the current range 0.2 to 1.3 mA.

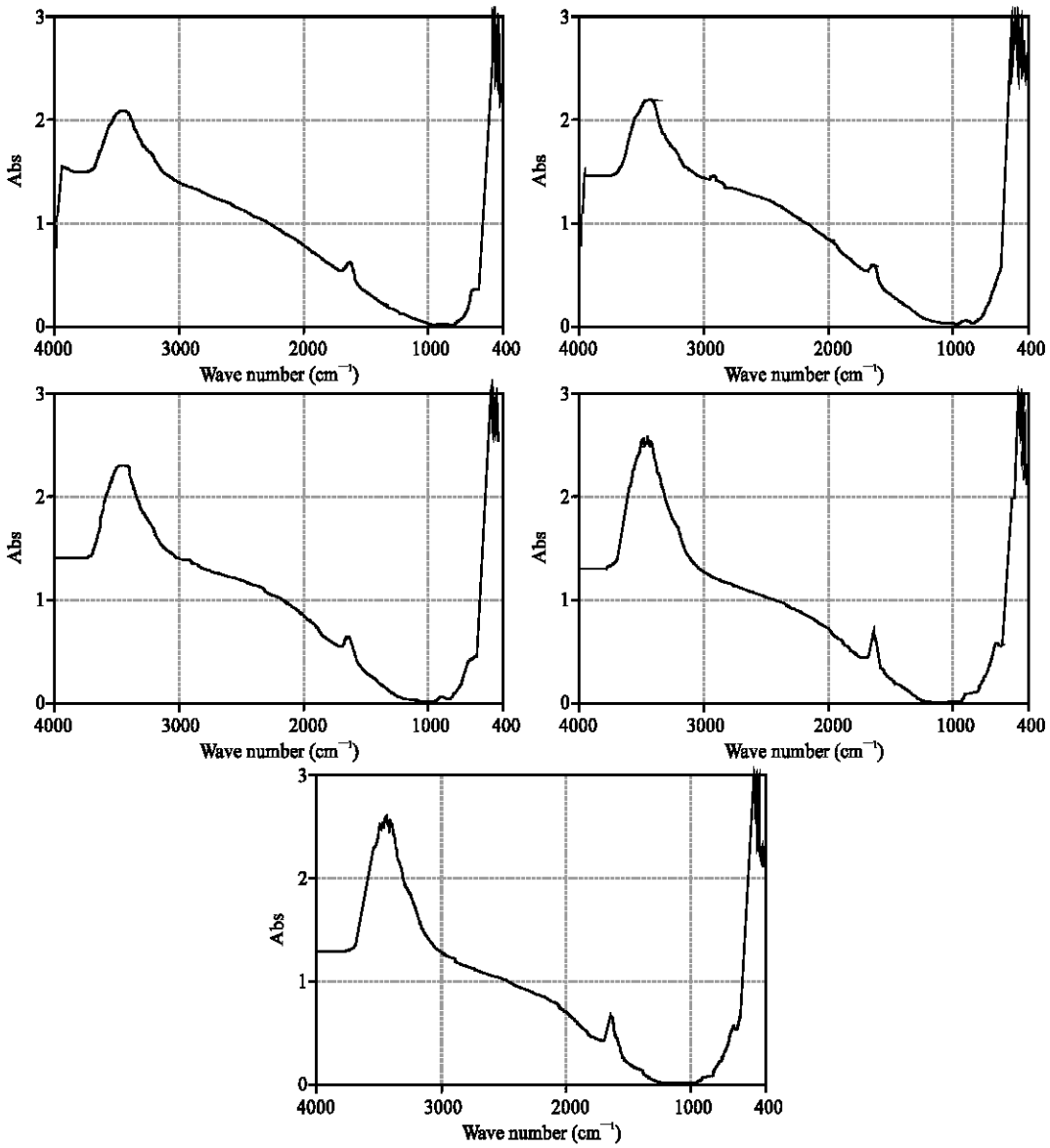

Fig. 8: FTIR spectra of Al doped ZBACS-based varistors samples sintered at 1200°C for 2 h with 1, 2, 3, 5 and 7 mol% of Al_2O_3 contents, from the top to the bottom, respectively

In Fig. 10, breakdown voltage (V_{BK}) and nonlinear coefficient (α) evaluated from the results of I-V measurement are presented as functions of Al_2O_3 content. The values of α (~1.8-3.0) are relatively low.

The electric conduction in the ohmic region was associated with the thermionic emission of Schottky type. For this type of mechanism the current density is related to the electric field and temperature by the Equation[1]:

$$J_s = A^*T^2 \exp\left[\left(\beta E^{1/2} - \phi_B\right)/k_B T\right]$$

where A* the effective Richardson constant. The theoretical value of the effective Richardson constant is given by

$$A^* = 4\pi m^* k^2 / h^3,$$

where h is the Plank constant, k is the Boltzmann constant and m* the electron effective mass for ZnO reported in the literature as 0.27 m_0[1], m_0 is the free electron mass. The theoretical value of A* = 32 A cm^{-2} K^2. ϕ_B The interface voltage barrier height, E is the electric field and β is a costant related to the potential barrier width by the relationship:

$$\beta \propto 1/\left(r^*\omega\right)$$

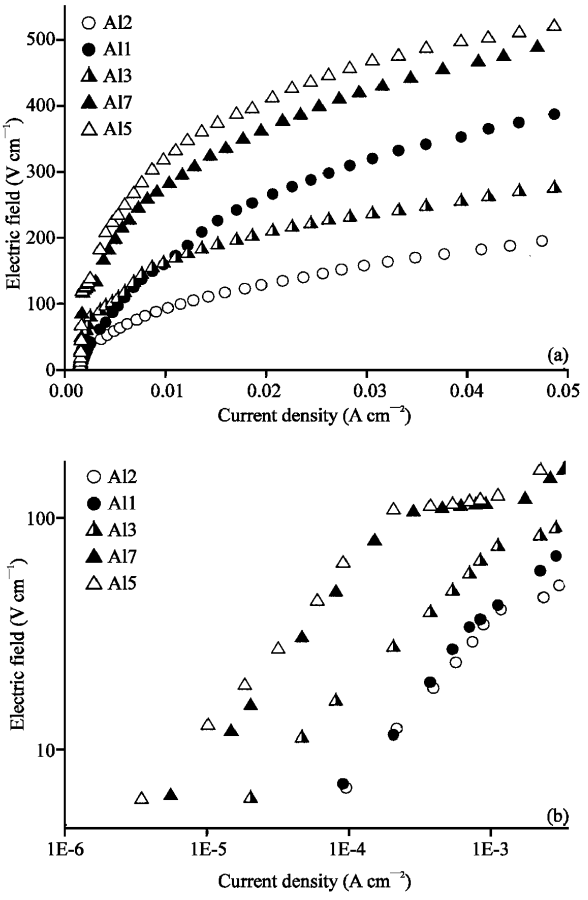

Fig. 9: The E-J characteristics of ZBACS-based varistors samples sintered at 1200°C for 2 h with Al_2O_3 content

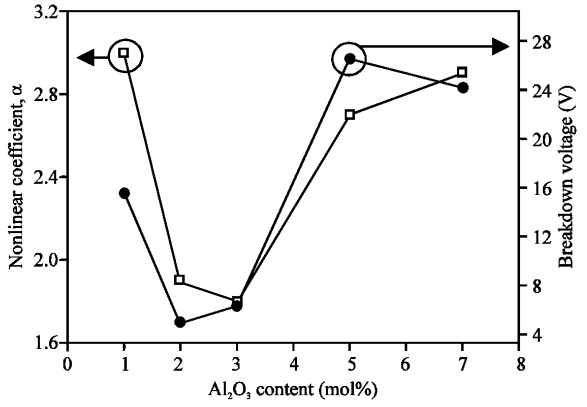

Fig. 10: Nonlinear coefficient (α) and breakdown voltage (V_{bk}) of ZBACS-based varistors samples as a function of Al_2O_3 content

Plots of lnJ against $E^{1/2}$ can be built up to determine values of ϕ_B, the interface voltage barrier height and ω a

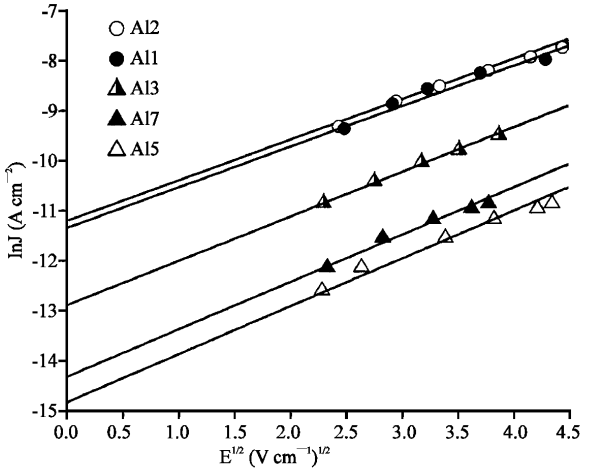

Fig. 11: Characteristic plots of ln J versus $E^{1/2}$ for samples with different Al_2O_3 content

Table 2: Some characteristics of the Al_2O_3-added $ZnO-Bi_2O_3$ based varistor samples

Al_2O_3 (mol.%)	V_{BK} (V)	α	$\ddot{O}_B$ (eV)	$\beta\times10^3$ ($eVcm^{1/2}V^{-1/2}$)
1	15.25	3.0	0.65	20
2	04.69	1.9	0.65	20
3	06.08	1.8	0.69	22
5	26.17	2.7	0.74	24
7	23.77	2.9	0.73	23

constant related to the potential barrier width, for the Al_2O_3-added $ZnO-Bi_2O_3$ based varistor, as shown in Fig. 11. ϕ_B Can be obtained from the intersection of the extrapolated lines of the plot with the lnJ axis and the relative magnitude of constant β, which is inverse to ω, the potential barrier width, can be derived from the slopes of the plots. Values of ϕ_B and β are shown in Table 2.

CONCLUSION

$ZnO-Bi_2O_3$-based varistor samples doped with 2.0 mol% of (Cr_2O_3+SiO_2) and varying amounts of Al_2O_3 in the range from 7.0 to 1.0 mol% were fired at 1200°C for 2h. A new process is described for achieving the current-voltage characteristics of a low voltage ZnO varistor. Microstructural and compositional of ZBACS-based varistors has been investigated. The sintered microstructure was less densified due to the increase of the fraction of $ZnAl_2O_4$ spinel phase as Al_2O_3 content increase and the increases in porosity which assigned to the evaporation of Bi_2O_3 during the liquid phase. Second phases, segregated and precipitated in ZnO-based varistors, encountered in triple junctions and grain boundaries regions were identified using XRD, SEM and energy dispersive spectrometry. The infra-red analysis reveals that the OH contents in the samples are

important. The hydrogen in Al doped ZBACS-based varistors may have a one site preference, resulting in a wider OH peak. The band at 662 cm^{-1} should be due to the presence of the $ZnAl_2O_4$ spinel. Addition of hydrogen to aluminium doped varistors slow down the grain growth effect.

ACKNOWLEDGEMENT

We would like to thank the research groups of Professor O. Khalfallah and N. Rouag of LMDM laboratory, Constantine state university, Algeria for their assistance in accomplishing this work.

REFERENCES

1. Gupta, T.K. and W.G. Calson, 1985. A grain-boundary defect model for instability/stability of a ZnO varistor, J. Mater. Sci., 20: 3487-3500.
2. Gupta, T.K., 1990. Application of ZnO oxide varistors, J. Am. Ceram. Soc., 73: 1817-1840.
3. Bowen, L.J. and F.J. Avella, 1983. Microstructure, electrical properties and failure prediction in low clamping voltage zinc oxide varistors, J. Applied Phys., 54: 2764-2772.
4. Hukuhara Y., 1983. J. Ceram. Soc. Jap., 91: 281.
5. Ghiotti, G., A. Chiorino and F. Boccuzzi, 1993. Surface chemistry and electronic effects of H_2 (D_2) on two different microcrystalline ZnO powders, Surf. Sci., 287: 228-234.
6. Van de Walle, C.G., 2000. Hydrogen as a cause of doping in zinc oxide, Phys. Rev. Lett., 85:1012-1015.
7. Cox, S.J.F., E.A. Davis, S.P. Cottrell, P.J.C. King, J.S. Lord and J.M. Gil *et al*., 2001. Experimental confirmation of the predicted shallow donor hydrogen state in zinc oxide, Phys. Rev. Lett., 86: 2601-2604.
8. Hofmann, D.M., A. Hofstaetter, F. Leiter, H. Zhou and F. Henecker *et al*., 2002. Hydrogen: A relevant shallow donor in zinc oxide, Phys. Rev. Lett., 88: 45504-45507.
9. Lavrov, E.V., J. Weber, F. Börrnert, C.G. Van de Walle, R. Helbig, 2002. Hydrogen-related defects in ZnO studied by infrared absorption spectroscopy, Phys. Rev. B, 66: 165205-165212.
10. Mollwo, E., 1954. Die Wirkung von Wasserstoff auf die Leitfähigkeit und Lumineszenz von Zinkoxydkristallen (The Effect of Hydrogen on the Conductivity and Luminescence of Zinc Oxide Crystals)," Z. Phys., 138: 478-488.
11. Thomas, D.G. and J.J. Lander, 1956. Hydrogen as a Donor in Zinc Oxide," J. Chem. Phys., 25: 1136-1142.
12. McCluskey, M.D., S.J. Jokela, K.K. Zhuravlev, P.J. Simpson and K.G. Lynn, 2002. Infrared Spectroscopy of Hydrogen in ZnO, Applied Phys. Lett., 81: 3807-3809.